TÜBİTAK

Turkish Journal of Earth Sciences

http://journals.tubitak.gov.tr/earth/

Research Article

Turkish J Earth Sci
(2016) 25: 434-455

doi:10.3906/yer-1605-4

Distribution of natural radioactivity and assessment of radioactive dose of Western Anatolian plutons, Turkey

Argyrios PAPADOPOULOS[1,*], Şafak ALTUNKAYNAK[2], Antonios KORONEOS[1], Alp ÜNAL[2], Ömer KAMACI[2]

[1]Department of Mineralogy, Petrology and Economic Geology, School of Geology, Aristotle University of Thessaloniki, Thessaloniki, Greece
[2]Department of Geological Engineering, Faculty of Mines, İstanbul Technical University, Maslak, İstanbul, Turkey

Received: 10.05.2016 • **Accepted/Published Online:** 28.06.2016 • **Final Version:** 24.10.2016

Abstract: The distribution of ^{226}Ra, ^{232}Th, and ^{40}K in 70 granite samples obtained from 13 Western Anatolian plutons (Turkey) was measured by using γ-ray spectroscopy. The activities of the measured radionuclides varied up to 259 Bq kg^{-1} for ^{226}Ra, up to 241 Bq kg^{-1} for ^{232}Th, and up to 2518 Bq kg^{-1} for ^{40}K, with mean values of 66 (±44), 90 (±47), and 1097 (±410) Bq kg^{-1}, respectively, which are smaller than the mean values given for granites worldwide. The mean value of the increase on the external γ-radiation effective dose rate is 0.21 (±0.09) mSv year^{-1}, varying by <1 mSv year^{-1}. The mean value of the internal α-radiation was 0.15 (±0.10) mSv year^{-1}, varying <0.5 mSv year^{-1}. Most of the samples cause an increase to both the external and internal dose by <30%, which is smaller than the permitted limit. Therefore, there is no radiological risk from the usage of the samples studied as decorative and ornamental building materials.

Key words: Building materials, Western Anatolia, granitic plutons, external–internal exposure, uranium, thorium, radiation index

1. Introduction

All varieties of building materials, including various naturally occurring as well as artificial materials, have varying concentrations of Ra, Th, and K and can cause direct radiation exposure to human beings. Granite, as a market term, includes a wide variety of rock types including plutonic, volcanic, and metamorphic rocks. Granite's durability and appearance make it a popular building material in dwellings. These rocks can contain various amounts of minerals with high Ra, Th, and K concentrations such as zircon, monazite, xenotime, allanite, epidote, or K-feldspars.

According to the European Commission (1999), radioactive doses should comply with the ALARA ("as low as reasonably achievable") radioprotection principle. The average annual effective equivalent should be limited to 1.6 mSv. Materials such as granites, potentially containing high concentrations of natural radionuclides, should be studied in order to control the exposure levels for human beings. The limit of 1.6 mSv per year is widely accepted by many international organisations such as the International Commission on Radiological Protection (ICRP), the World Health Organization (WHO), and the European Commission.

Natural radionuclides increase both the external (γ-rays) and internal (α-rays) radiation to human beings. ^{238}U, ^{232}Th, and ^{40}K are the main contributors of γ-rays, while α-rays are principally emitted by radon, a decay product of ^{238}U radioactive series. The Rn isotopes are responsible for roughly half of the radioactive dose exposure from natural sources. Moreover, Rn isotopes are considered as an important cause of lung cancer (UNSCEAR, 2000; WHO, 2009).

Many investigations on the radioactivity levels of granitic rocks, used or potentially used as decorative and building materials, can be found in the recent literature (Tzortzis et al., 2003; Anjos et al., 2005; Örgün et al., 2005, 2007; Salas et al., 2006; Mao et al., 2006; Pavlidou et al., 2006; Xinwei et al., 2006; Kitto et al., 2009; Anjos et al., 2011; Karadeniz et al., 2011; Marocchi et al., 2011; Moura et al., 2011; Amin, 2012; Cetin et al., 2012; Papadopoulos et al., 2012, 2013; Turhan, 2012; Iwaoka et al., 2013; Karadeniz and Akal, 2014; Angi et al., 2016; Erkul et al., 2016). Japan, Brazil, Italy, the United States, and China are the dominating countries of the granite trade worldwide. This means that most granites used as building materials originate from these countries.

In this study, we demonstrate the distribution of natural radioactivity of the most important Western Anatolian granitic plutons in Turkey and we assess any possible health risk if they were to be used as construction materials. The necessary radiation indices were calculated

* Correspondence: argpapad@geo.auth.gr

and the data were statistically treated with Pearson's correlation coefficients and principal component analysis (PCA).

2. Materials and methods

2.1. Geological setting

The Cenozoic geology of Western Anatolia (Turkey) is characterised by intensive magmatic activity producing volcanic and plutonic rocks. The latter can be mainly used as decorative building materials (Figure 1). The geology, petrology, geochronology, and tectonic setting of these magmatic rocks have been studied in detail previously by various researchers. Hence, we refer the interested reader to the previous papers on these topics (i.e. Şengör and Yılmaz, 1981; Yılmaz, 1989; Güleç, 1991; Harris et al., 1994; Altunkaynak and Yılmaz, 1998; Aldanmaz et al., 2000; Okay and Satır, 2000, 2006; Köprübaşı and Aldanmaz, 2004; Altunkaynak and Dilek, 2006, 2013; Dilek and Altunkaynak, 2007, 2010; Altunkaynak and Genç, 2008; Boztuğ et al., 2009; Ersoy et al., 2009; Erkül, 2010, 2012; Hasözbek et al., 2010; Altunkaynak et al., 2010, 2012a, 2012b; Erkül and Erkül, 2012; Erkül et al., 2013).

In Western Anatolia, following the closure of the Neo-Tethyan Ocean, postcollisional magmatic activity producing granitic plutons developed in two phases which climaxed in the Eocene and Oligo-Miocene. The first episode of magmatism produced mostly I-type granitoids and associated extrusive rocks that are medium-K and high-K calc-alkaline in composition (Harris et al., 1994; Koprubasi and Aldanmaz, 2004; Altunkaynak, 2007;

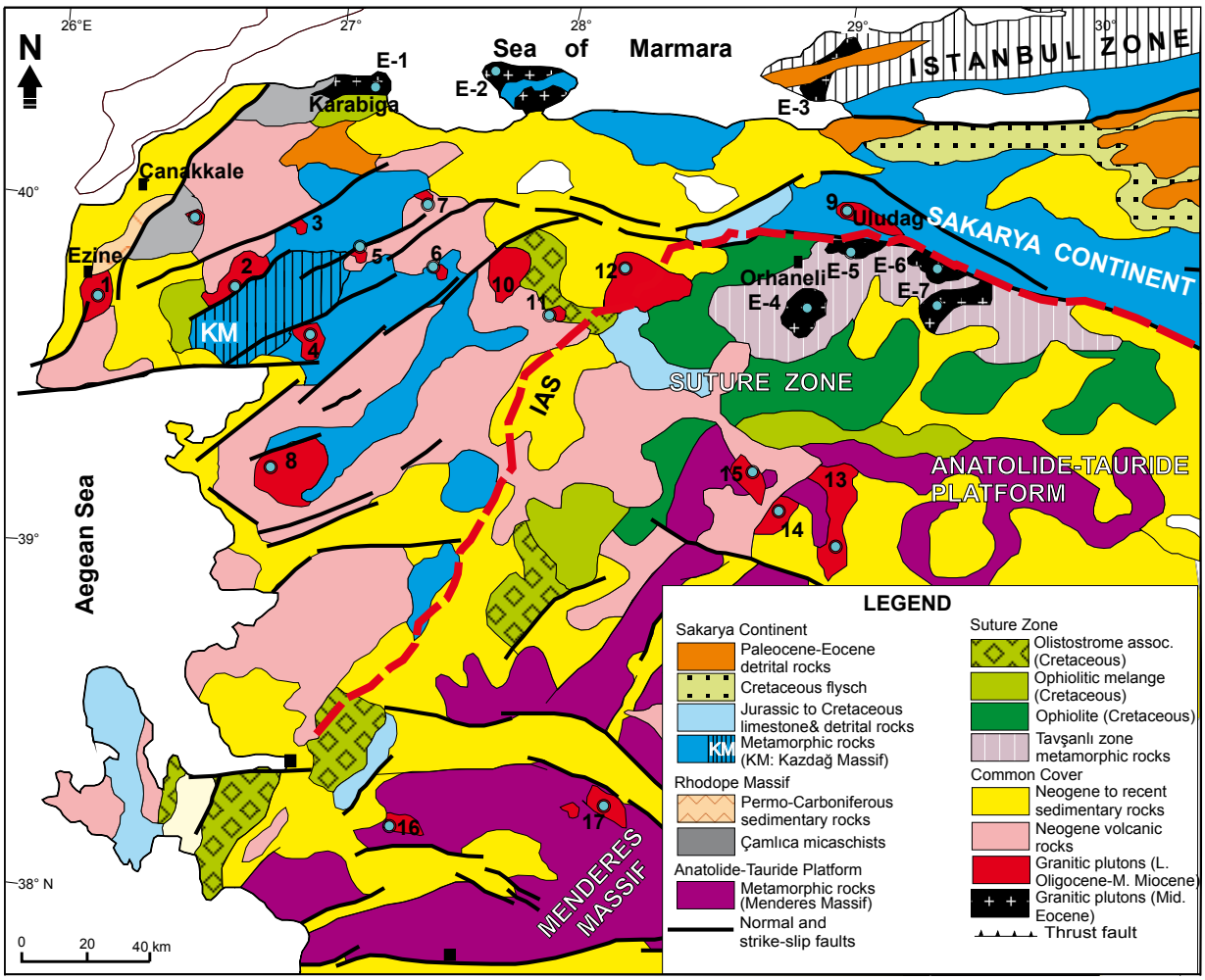

Figure 1. Simplified geological map of western Anatolia showing the distribution of the studied granitoids (modified from Yılmaz et al., 2000; Okay and Satır, 2006; Altunkaynak et al., 2012a). IAS: İzmir-Ankara-Erzincan suture zone. E1 to E7: Eocene granitoids (E1: Karabiga, E2: Kapıdağ, E3: Fıstıklı, E4: Orhaneli, E5: Topuk, E6: Göynükbelen, E7: Gürgenyayla). 1 to 15: Oligo-Miocene granitoids (1- Kestanbol, 2- Evciler, 3- Hıdırlar-Katrandag, 4- Eybek, 5- Yenice, 6- Danişment, 7- Sarıoluk, 8- Kozak, 9- Uludağ, 10- Ilıca-Şamlı, 11- Davutlar, 12- Çataldağ, 13- Eğrigöz, 14- Koyunaoba, 15- Çamlik, 16- Turgutlu, 17- Salihli granitoids).

Altunkaynak et al., 2012a). The Eocene granitic plutons occurred within the İzmir-Ankara Suture Zone (IASZ) and Sakarya Continent (SC). Among these, Orhaneli, Topuk, and Gürgenyayla plutons were exposed along the IASZ and intruded into the Cretaceous blueschist rocks and overlying ophiolitic units. They range in composition from quartz diorite and granodiorite to syenite. Fıstıklı (Armutlu), Karabiga, and Kapıdağ plutons, on the other hand, crop out along the southern margin of the Sea of Marmara. These plutons intruded into the crystalline basement rocks of the SC to the north of the IASZ. They are composed of monzogranite, granodiorite, and granite and their subordinate hypabyssal and extrusive counterparts. The second magmatic phase generated voluminous granitic plutons (i.e. Kestanbol, Uludağ, Çataldağ, Kozak, Ilıca, Eğrigöz, Evciler, Çamlık, and Eybek) and extrusive rocks mostly high-K calc-alkaline and shoshonitic in character. Oligo-Miocene granitic plutons and associated volcanic rocks are widespread in the entire West Anatolia (Yilmaz, 1989; Yilmaz et al., 2001; Altunkaynak et al., 2012a, 2012b; Ozgenc and Ilbeyli, 2008; Akay, 2009). The Çataldağ, Kozak, Ilıca, Evciler, and Eybek granitoids intruded into the crystalline basement rocks of the SC. The Koyunoba, Çamlık, and Eğrigöz plutons, on the other hand, were intrusive into the metamorphic basement rocks of the Anatolide-Tauride Platform (Altunkaynak and Dilek, 2006; Erkül, 2010; Altunkaynak et al., 2012b; Erkül and Erkül, 2012). Most of the Oligo-Miocene granites are represented by caldera-type shallow level intrusions presenting spatial and temporal relationships with their volcanic and subvolcanic counterparts (Yılmaz, 1989; Altunkaynak and Yilmaz, 1998, 1999; Genç, 1998; Yılmaz et al., 2001).

2.2. Gamma-ray spectroscopy

The measurements for natural radioactivity levels were undertaken in the Low Level Radioactivity Measurement Laboratory of the İstanbul Technical University Energy Institute by using a copper-lined lead shielding (10 cm) detector (GAMMA-X HPGe coaxial n-type germanium detector, 45.7 % efficiency and 1.84 keV full width at half maximum for 1.3 MeV of ^{60}Co) with an integrated digital gamma spectrometer (DSPEC jr. 2.0). Statistical confidence level and range were adjusted to 2σ and 8K, respectively. Samples and a standard in Marinelli beakers were counted at the top of the detector. Counting times were adjusted to 15 to 24 h. Peak areas were determined by using the GAMMA VISION-32 software program.

In order to make the energy and efficiency calibrations of the gamma spectroscopy system that are necessary for activity determination, a certificated multiple gamma-ray emitting large volume source standard was used including ^{241}Am, ^{137}Cs, ^{60}Co, ^{210}Pb, ^{109}Cd, ^{57}Co, ^{139}Ce, ^{203}Hg, ^{113}Sn, ^{85}Sr, and ^{88}Y radioisotopes in the sand matrix in Marinelli geometry as 500 mL volume, with a density of 1.7 g cm^{-3} and an activity of 1 μCi.

The full-energy peak detection efficiencies for source radionuclide energies were obtained by

$$\varepsilon = \frac{N_p}{t_m \cdot A \cdot \gamma}$$

where N_p is net photopeak count, t_m is measurement time (s), g is the gamma-emission probability, and A is the gamma-emission rate that has to be calculated from the certified source activity (in disintegrations/s) considering the time elapsed from the calibration of the source to the time of its use (Debertin and Helmer, 1988; Gilmore, 2008). The efficiency-curve approach was then applied and the efficiencies for selected radionuclide energies of samples were obtained from the fitting equation

$$\log \varepsilon = \sum_{i=0}^{n} a_i \cdot \log^i (E)$$

of the efficiency curve (Figure 2).

Considering the attenuation effect of different densities of samples at different energies to count rates, the direct transmission method proposed by Cutshall et al. (1983) was applied. Pluton samples were grouped according to their densities and the measurements were applied for selected densities with different energetic point sources. For this reason the point sources were placed one after another on the top of an empty Marinelli beaker and also on Marinelli beaker containers filled with pluton samples and counted for 1000 s. The relative self-correction factor f_{att} for a sample $f_{att;s}$ with respect to a standard sample $f_{att;std}$ was determined by an equation adapted from Robu and Giovani (2009):

$$f_{att} = \frac{f_{att;\,s}}{f_{att;\,std}} = \left(\frac{(\ln I / I_0)}{(1-(I/I_0))} \right)_{att;\,s} \Bigg/ \left(\frac{(\ln I / I_0)}{(1-(I/I_0))} \right)_{att;\,std}$$

where I and I_0 are the peak count rates for the samples and empty Marinelli beakers with the point source. Attenuation coefficients for measured radionuclide energies were obtained from the attenuation coefficient to density curves given in Figure 3.

Radioactivity concentrations of samples were calculated as:

$$a = \frac{(n_{N,E} / t_g)}{(P_E \cdot \varepsilon_E \cdot m \cdot f_E \cdot f_{att;\,s,\,std})}$$

where a signifies the activity per unit of mass of each radionuclide present in the sample, $n_{N,E}$ denotes the

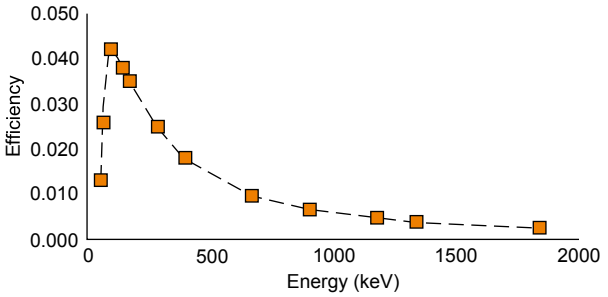

Figure 2. Efficiency curve.

number of counts in the net area of the peak at energy E in the sample spectrum with background correction, t_g symbolises the sample spectrum counting time, P_E corresponds to the probability of the emission of gamma-radiation with energy E for each radionuclide, m is a symbol of the mass of the test portion, and $f_{att;s,\ std}$ is the relative self-correction factor.

The results of the gamma-ray spectroscopy measurements are given in Table 1.

2.3. Major elements

The major element contents of 70 samples are given in Table 2. The whole-rock major element compositions of granitic rocks were determined by Spectro Ciros Vision ICP-ES for major oxides at ACME Labs (Canada).

2.4. Rock types and mineralogical composition

All the samples have been examined under a polarised microscope to identify the mineralogical composition. As shown in Figure 4, a variety of rock types, from quartz monzodiorite to syenogranite, have been studied. Hornblende, biotite, and muscovite are the major mineral constituents. The accessory minerals present are zircon, apatite, titanite, allanite, chlorite, monazite, garnet, and epidote. The rock type, the colour, the grain size, and the mineralogical composition are presented in Table 3.

Selected polished sections were analysed by using the SEM-EDS JEOL JSM840A-INCA 300 at the Scanning Microscope Laboratory, Aristotle University of Thessaloniki. Operating conditions were: accelerating voltage 20 kV, probe current 45 nA, and counting time 60 s.

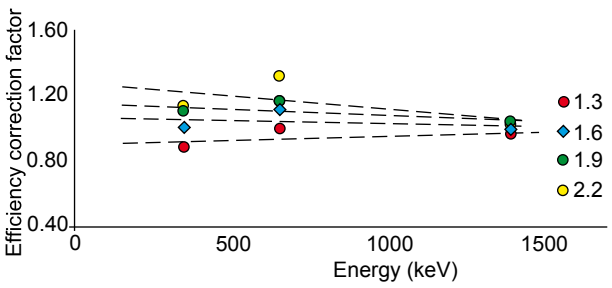

Figure 3. Attenuation coefficients versus energy plots.

Some euhedral grains of the studied minerals are shown in Figure 5.

3. Results

3.1. Concentration of natural radionuclides

The activities of the natural radionuclides measured in the granites studied varied up to 259 Bq kg^{-1} for ^{226}Ra, up to 241 Bq kg^{-1} for ^{232}Th, and up to 2518 Bq kg^{-1} for ^{40}K, with a mean value of 66 (±44), 90 (±47), and 1097 (±410) Bq kg^{-1}, respectively. Strong and statistically significant correlations were found between the radionuclides studied, implying that ^{226}Ra and ^{232}Th have similar geochemical behaviour and concentrate with the same mechanisms in igneous rocks. In contrast, they both have negative correlations with ^{40}K, which has quite different geochemical characteristics. Moreover, strong and significant correlations are also present between the radionuclides and the K_2O/SiO_2 molecular ratio (Table 4). This suggests that the excess of K_2O over SiO_2 in magma causes the elements with large ionic radius and charge (e.g., U and Th) to be more soluble; therefore, their concentration in minerals and rocks is increased.

The ^{226}Ra and ^{232}Th activities of the majority of the Western Anatolian granites are below the mean values of 78 and 111 Bq kg^{-1} reported by UNSCEAR (1993), by 80% and 77.1%, respectively (Table 5). On the other hand, 55.7%, 24.4%, and 2.85% of the samples of this study have lower ^{226}Ra, ^{232}Th, and ^{40}K activities than the average of building materials given by UNSCEAR (1993).

Comparing the average specific activities of ^{226}Ra and ^{232}Th of the Western Anatolian samples (70 samples) with imported ones in the SE Mediterranean countries (Greece, Cyprus, and Egypt. 194 samples), it can be concluded that they are quite similar. However, it must be noted that ^{226}Ra concentrations of the raw granites from Western Anatolia are quite smaller than those of the imported ones in Turkey.

The average ^{40}K of the studied samples and the most popular commercial granites (hereafter PCG) originating from Japan, Italy, the United States, and Brazil are similar. Excepting the US (Kitto et al., 2009) and Japanese (Iwaoka et al., 2013) granites, the average ^{232}Th of the Western Anatolian granites is lower than that of the PCG. Comparing the PCG and the average ^{226}Ra of the Western Anatolian granites, the samples studied have smaller concentrations. Therefore, the Western Anatolian granites, at least from a radioactivity level point of view, are comparable to the PCG. An estimation of radioactivity indices and doses is necessary aiming to support what is mentioned above.

3.2. Estimations of radioactivity indices and doses

Both external exposure (γ-rays emitted by the radioactive decay of ^{40}K, ^{226}Ra, and ^{232}Th) and internal exposure (α-particles emitted by the inhaled Rn indoors) can be

Table 1. Activities of ^{226}Ra, ^{232}Th, and ^{40}K in the Western Anatolian granites. (bdl = below detection limit, ND = not detected)

		^{226}Ra		^{232}Th		^{40}K	
	Pluton name	Activity (Bq/kg)	Uncertainty (%)	Activity (Bq/kg)	Uncertainty (%)	Activity (Bq/kg)	Uncertainty (%)
AS209	Ilıca	86.18	4.98	90.08	3.16	2080.97	0.70
AS211	Ilıca	83.54	10.91	194.14	3.48	1455.02	1.69
AS234	Ilıca	37.30	24.73	136.99	2.06	1115.14	0.84
AS236	Ilıca	111.08	5.44	0.14	1.57	1083.97	0.65
AS238	Ilıca	105.91	2.65	179.68	1.09	1219.12	0.77
AS239	Ilıca	65.39	3.36	124.87	1.33	1239.06	1.01
AS240	Ilıca	67.51	2.79	107.20	2.13	995.59	0.76
AS241	Ilıca	113.66	6.59	140.47	1.97	1250.15	1.49
AS245	Ilıca	47.35	12.05	99.04	1.60	1230.46	0.97
AS248	Ilıca	53.06	3.00	93.59	2.11	889.87	0.74
Average		77.10	7.65	116.62	2.05	1255.93	0.96
St. dev.		27.33	6.86	53.99	0.76	328.94	0.35
Min		37.30	2.65	0.14	1.09	889.87	0.65
Max		113.66	24.73	194.14	3.48	2080.97	1.69
ÇAT1	Çataldağ	150.97	3.48	131.91	1.38	1061.14	0.85
ÇAT2	Çataldağ	259.47	1.37	139.84	3.45	1972.34	0.65
ÇAT3	Çataldağ	99.35	2.55	118.51	1.48	1348.36	0.68
ÇAT4	Çataldağ	116.35	2.27	148.00	1.25	1425.66	0.66
ÇAT5	Çataldağ	44.15	4.13	95.67	1.59	1027.22	0.85
ÇAT6	Çataldağ	61.87	3.93	26.36	11.32	804.17	1.91
OS388	Çataldağ	176.84	1.70	176.37	4.95	1669.11	0.65
OS409	Çataldağ	83.63	3.55	72.95	3.03	1752.08	1.05
Average		124.08	2.87	113.70	3.56	1382.51	0.91
St. dev.		70.11	1.04	47.44	3.40	402.43	0.43
Min		44.15	1.37	26.36	1.25	804.17	0.65
Max		259.47	4.13	176.37	11.32	1972.34	1.91
ULU3	Uludağ	64.83	2.86	76.83	2.99	951.90	0.84
ULU5	Uludağ	80.53	2.74	104.17	1.64	1239.83	0.79
ULU6	Uludağ	80.38	2.75	115.26	4.55	1223.74	0.96
ULU8	Uludağ	104.06	2.14	77.17	3.53	994.77	0.33
ULU11	Uludağ	105.05	2.25	78.61	2.00	1125.87	0.83
ULU12	Uludağ	78.20	3.76	70.89	5.06	1101.88	1.20
Average		85.51	2.75	87.16	3.29	1106.33	0.83
St. dev.		15.86	0.58	18.02	1.36	116.88	0.28
Min		64.83	2.14	70.89	1.64	951.90	0.33
Max		105.05	3.76	115.26	5.06	1239.83	1.20
EYB10	Eybek	35.18	10.95	49.85	8.67	681.12	1.69
EYB14	Eybek	48.51	3.43	55.98	3.01	782.48	1.60
EYB15	Eybek	41.44	14.42	67.08	2.97	759.89	1.46

Table 1. (Continued).

EYB24	Eybek	ND	ND	39.27	2.67	481.84	1.25
EYB30	Eybek	41.40	5.77	48.68	3.63	591.48	1.63
EYB34	Eybek	38.31	7.69	76.74	5.47	845.23	1.89
EYB35	Eybek	32.15	6.55	61.70	3.04	723.73	1.50
EYB38	Eybek	49.82	3.82	81.37	1.78	737.28	1.03
Average		40.97	7.52	60.08	3.91	700.38	1.51
St. dev.		6.50	3.95	14.47	2.19	115.36	0.27
Min		32.15	3.43	39.27	1.78	481.84	1.03
Max		49.82	14.42	81.37	8.67	845.23	1.89
KOZ1	Kozak	60.62	3.68	109.26	3.16	1215.47	0.87
KOZ2	Kozak	55.35	11.78	104.91	3.63	1200.75	0.82
KOZ4	Kozak	68.75	6.62	96.65	1.65	1203.40	0.78
KOZ5	Kozak	104.64	8.23	124.85	2.13	1274.24	1.07
KOZ8	Kozak	69.81	4.38	152.18	2.90	1484.56	0.96
KOZ9	Kozak	59.16	3.29	116.30	1.41	1468.41	0.67
KOZ10	Kozak	ND	ND	133.25	2.06	1253.34	1.05
Average		69.72	6.33	119.63	2.42	1300.03	0.89
St. dev.		18.01	3.27	18.87	0.82	123.55	0.15
Min		bdl	-	96.65	1.41	1200.75	0.67
Max		104.64	3.29	152.18	3.63	1484.56	1.07
EVC1	Evciler	ND	ND	78.23	5.84	917.44	1.53
EVC2	Evciler	51.18	5.87	106.52	4.37	1249.60	1.37
EVC3	Evciler	72.25	4.30	107.40	3.21	1045.38	1.32
EVC5	Evciler	101.78	5.16	136.80	3.57	810.46	2.08
EVC6	Evciler	ND	ND	155.40	1.87	1076.98	0.78
EVC8	Evciler	ND	ND	150.24	1.62	147.84	2.87
Average		225.21	15.33	122.43	3.41	874.62	1.66
St. dev.		25.42	0.79	30.00	1.58	385.97	0.73
Min		bdl	-	78.23	1.62	147.84	0.78
Max		101.78	5.87	155.40	5.84	1249.60	2.87
ORH1	Orhaneli	18.94	8.02	31.57	5.82	738.87	1.64
ORH3	Orhaneli	18.11	5.78	30.59	4.53	810.22	1.09
ORH5	Orhaneli	18.50	9.65	39.09	6.79	698.12	1.44
ORH6	Orhaneli	141.34	4.98	240.63	2.38	2517.80	0.65
Average		49.22	7.11	85.47	4.88	1191.25	1.21
St. dev.		61.41	2.13	103.51	1.90	885.58	0.43
Min		18.11	4.98	30.59	2.38	698.12	0.65
Max		141.34	9.65	240.63	6.79	2517.80	1.64
KAP42	Kapıdağ	20.30	5.06	52.82	3.11	1072.85	0.75
KAP43	Kapıdağ	46.96	3.69	48.08	2.94	1442.38	0.82
KAP45	Kapıdağ	20.48	6.41	61.40	2.07	876.94	0.98
KAP46	Kapıdağ	13.28	7.70	17.83	10.35	388.16	2.09

Table 1. (Continued).

KAP47	Kapıdağ	24.82	5.55	66.84	1.87	587.24	1.21
KAP52	Kapıdağ	69.78	2.86	15.67	8.96	1081.01	1.19
Average		32.60	5.21	43.77	4.88	908.10	1.17
St. dev.		21.54	1.77	21.93	3.75	378.62	0.49
Min		13.28	2.86	15.67	1.87	388.16	0.75
Max		69.78	7.70	66.84	10.35	1442.38	2.09
CAM28	Çamlık	ND	ND	69.19	6.36	1392.46	1.11
CAM29	Çamlık	ND	ND	80.60	3.30	1582.49	1.66
CAM30	Çamlık	75.19	4.15	81.89	2.81	1053.51	1.26
Average		75.19	4.15	77.23	4.16	1342.82	1.34
St. dev.		-	-	6.99	1.92	267.96	0.28
Min		bdl	-	69.19	2.81	1053.51	1.11
Max		75.19	4.15	81.89	6.36	1582.49	1.66
TOP9	Topuk	59.67	3.40	74.60	2.07	909.90	0.92
TOP11	Topuk	ND	ND	41.97	3.43	641.52	1.79
TOP12	Topuk	20.86	11.11	69.19	1.94	995.98	0.99
Average		40.27	7.26	61.92	2.48	849.13	1.23
St. dev.		27.44	5.45	17.49	0.83	184.88	0.48
Min		bdl	-	41.97	1.94	641.52	0.92
Max		59.67	4.15	74.60	3.43	995.98	1.79
TPL1	Tepeldağ	ND	ND	134.70	1.86	1732.01	1.73
TPL13	Tepeldağ	23.75	6.64	79.81	2.00	1374.73	0.79
TPL14	Tepeldağ	13.34	6.42	20.95	5.31	410.72	1.22
Average		18.55	6.53	78.49	3.06	1172.49	1.25
St. dev.		7.36	0.16	56.89	1.95	683.47	0.47
Min		bdl	-	20.95	1.86	410.72	0.79
Max		23.75	6.64	134.70	5.31	1732.01	1.73
GÜR18	Gürgenyayla	24.46	11.45	22.15	9.01	898.99	1.45
GÜR19	Gürgenyayla	ND	ND	42.31	4.62	554.85	1.29
GÜR20	Gürgenyayla	29.08	4.56	45.59	5.08	615.65	1.11
Average		26.77	8.01	36.68	6.24	689.83	1.28
St. dev.		3.27	4.87	12.70	2.41	183.67	0.17
Min		bdl	-	22.15	4.62	554.85	1.11
Max		29.08	11.45	45.59	9.01	898.99	1.45
EGR23	Eğrigöz	47.29	6.15	75.83	3.16	1255.73	1.21
EGR24	Eğrigöz	55.54	8.51	73.83	2.04	1403.31	0.87
EGR27	Eğrigöz	38.34	4.58	105.48	1.50	1545.88	0.66
Average		47.06	6.41	85.05	2.23	1401.64	0.91
St. dev.		8.60	1.98	17.73	0.85	145.08	0.28
Min		38.34	4.58	73.83	1.50	1255.73	0.66
Max		55.54	8.51	105.48	3.16	1545.88	1.21

Table 2. Major element content (% wt.) of the studied samples.

	SiO_2	TiO_2	Al_2O_3	Fe_2O_3	MnO	MgO	CaO	Na_2O	K_2O	P_2O_5	LOI	Sum
AS209	65.17	0.47	15.41	4.45	0.08	1.96	4.08	3.23	3.68	0.19	0.90	99.62
AS211	67.09	0.40	15.42	3.82	0.10	1.54	3.90	3.45	3.11	0.15	0.70	99.68
AS234	65.31	0.47	15.20	4.56	0.09	2.09	4.56	3.33	3.13	0.21	0.70	99.65
AS236	64.26	0.49	15.94	4.42	0.08	2.08	4.43	3.37	3.67	0.19	0.70	99.63
AS238	63.00	0.50	16.60	4.88	0.10	1.95	4.82	3.59	2.94	0.22	1.10	99.70
AS239	62.42	0.57	15.84	5.42	0.11	2.68	5.01	3.42	2.91	0.18	1.10	99.66
AS240	62.71	0.52	16.16	4.78	0.10	2.25	4.51	3.38	3.18	0.16	1.90	99.65
AS241	62.40	0.53	16.64	5.07	0.10	2.30	5.39	3.44	2.75	0.20	0.80	99.62
AS245	62.75	0.56	16.21	5.33	0.10	2.64	5.13	3.37	2.89	0.16	0.50	99.64
AS248	63.51	0.50	16.08	4.77	0.09	2.21	4.65	3.46	3.07	0.17	1.20	99.71
ÇAT1	68.90	0.27	15.06	3.10	0.07	0.82	2.58	3.10	4.22	0.11	2.05	100.28
ÇAT2	74.51	0.03	13.68	0.63	0.16	0.05	1.08	4.43	3.56	<0.01	0.70	98.83
ÇAT3	68.02	0.38	14.75	3.17	0.07	0.99	2.51	3.46	4.04	0.14	1.01	98.53
ÇAT4	67.68	0.35	15.49	3.25	0.09	0.77	3.36	4.08	2.94	0.17	0.70	98.87
ÇAT5	73.57	0.04	14.29	0.66	0.03	0.22	1.11	3.45	4.06	0.08	1.89	99.40
ÇAT6	77.25	0.04	13.58	0.45	0.02	0.11	0.82	3.76	3.92	0.06	0.86	100.88
OS388	73.34	0.22	15.10	1.71	0.04	0.43	2.09	3.90	3.17	0.07	1.01	101.08
OS409	72.64	0.09	14.88	0.80	0.01	0.19	1.12	3.63	5.37	0.09	1.10	99.92
ULU3	71.39	0.26	15.39	1.72	0.04	0.73	2.16	4.26	2.73	0.12	0.90	99.70
ULU5	71.08	0.27	15.65	1.56	0.02	0.52	1.75	3.97	3.63	0.11	1.10	99.66
ULU6	71.67	0.26	15.14	1.59	0.03	0.63	2.08	4.21	3.20	0.11	0.80	99.72
ULU8	71.91	0.23	15.30	1.37	0.03	0.48	1.82	4.08	3.41	0.10	1.00	99.73
ULU11	71.42	0.25	15.13	1.52	0.03	0.63	2.01	4.11	3.28	0.11	1.30	99.79
ULU12	72.03	0.24	15.25	1.44	0.03	0.50	1.36	3.96	3.91	0.13	0.90	99.75
EYB10	58.26	0.68	17.53	6.90	0.14	3.05	6.96	3.91	1.61	0.17	0.50	99.71
EYB14	60.41	0.69	16.22	6.50	0.13	3.00	5.39	3.75	2.17	0.14	1.30	99.70
EYB15	63.10	0.64	16.02	5.62	0.11	2.31	5.33	3.63	1.94	0.14	0.90	99.74
EYB24	61.18	0.52	17.21	5.19	0.11	1.80	4.48	4.80	1.49	0.12	2.80	99.70
EYB30	58.13	0.79	17.05	7.25	0.14	3.41	6.72	3.65	1.66	0.18	0.70	99.68
EYB34	60.73	0.66	16.72	6.28	0.13	2.40	5.33	3.76	2.09	0.15	1.40	99.65
EYB35	61.80	0.58	16.52	5.69	0.12	2.22	5.05	3.64	2.40	0.14	1.50	99.66
EYB38	61.19	0.66	16.52	6.14	0.12	2.60	5.67	3.67	2.01	0.15	1.00	99.73
KOZ1	66.01	0.42	16.09	3.61	0.06	1.58	3.50	3.62	3.40	0.16	1.20	99.65
KOZ2	63.04	0.53	16.08	4.32	0.07	2.29	4.38	3.47	3.58	0.22	1.70	99.68
KOZ4	64.60	0.51	15.62	4.02	0.07	2.27	4.05	3.35	3.77	0.20	1.10	99.56
KOZ5	71.44	0.29	14.47	2.14	0.05	0.64	2.16	3.59	4.15	0.09	0.60	99.62
KOZ8	65.32	0.51	15.73	4.00	0.07	2.18	3.98	3.41	3.84	0.21	0.40	99.65
KOZ9	64.19	0.50	16.18	4.14	0.07	2.21	4.16	3.53	3.90	0.22	0.50	99.60
KOZ10	65.63	0.49	15.37	3.94	0.07	2.14	3.83	3.27	3.85	0.21	0.80	99.60
EVC1	61.99	0.57	16.73	5.78	0.10	2.41	4.95	3.36	2.83	0.16	0.80	99.68
EVC2	64.06	0.49	15.94	4.90	0.11	1.95	4.47	3.37	2.87	0.13	1.50	99.79
EVC3	63.68	0.50	16.40	5.04	0.11	1.94	4.71	3.50	2.76	0.12	1.00	99.76

Table 2. (Continued).

EVC5	65.38	0.44	15.43	4.28	0.10	1.94	4.03	3.22	3.77	0.17	0.90	99.66
EVC6	64.42	0.45	15.67	4.50	0.10	2.02	4.39	3.27	3.45	0.18	1.20	99.65
EVC8	66.69	0.41	15.12	1.69	0.06	2.14	4.80	4.01	0.47	0.16	4.20	99.75
ORH1	63.47	0.39	17.24	4.60	0.09	1.80	5.39	3.74	2.17	0.10	0.67	99.66
ORH3	63.81	0.38	17.44	4.29	0.09	1.66	5.16	4.01	1.98	0.12	0.71	99.64
ORH5	65.50	0.32	17.05	3.44	0.08	1.36	4.80	3.94	2.05	0.10	0.93	99.57
ORH6	64.93	0.37	16.59	2.76	0.06	0.77	2.00	4.77	6.42	0.12	1.08	99.87
KAP42	71.61	0.23	14.60	2.06	0.07	0.51	2.57	3.71	3.10	0.04	0.81	99.31
KAP43*	71.54	0.19	14.21	1.99	0.08	0.51	2.26	3.39	3.38	0.06	1.78	99.40
KAP45	64.18	0.50	16.83	4.78	0.10	1.84	5.12	3.54	2.15	0.10	0.48	99.64
KAP46	63.43	0.51	16.19	4.76	0.09	2.25	4.83	3.43	3.16	0.16	0.80	99.61
KAP47*	63.30	0.61	16.15	5.43	0.13	2.01	5.11	3.14	2.12	0.11	0.85	98.97
KAP52*	69.17	0.27	16.02	2.43	0.07	0.53	3.41	4.39	2.30	0.07	0.62	99.27
CAM28*	71.99	0.21	14.35	1.86	0.06	0.59	1.77	3.29	4.12	0.09	1.21	99.56
CAM29*	68.63	0.31	15.40	2.91	0.04	1.01	2.61	2.52	5.07	0.17	0.64	99.32
CAM30*	65.20	0.44	16.66	4.00	0.05	1.50	3.75	3.68	3.26	0.25	0.80	99.59
TOP9	64.55	0.38	16.59	4.34	0.14	1.40	5.26	3.77	1.88	0.12	0.67	99.09
TOP11	66.49	0.34	16.83	3.67	0.11	0.99	4.93	3.99	1.73	0.11	0.44	99.64
TOP12	67.37	0.29	16.44	3.32	0.10	1.05	4.37	3.38	2.71	0.08	0.70	99.81
TPL1	61.16	0.60	16.79	5.73	0.13	2.15	5.41	4.18	1.89	0.16	0.92	99.12
TPL13*	70.20	0.28	14.51	2.60	0.08	0.92	2.73	4.27	3.50	0.05	0.61	99.75
TPL14	54.94	0.76	17.37	7.39	0.15	4.52	8.63	3.42	1.19	0.16	0.89	99.42
GÜR18*	64.00	0.48	16.00	4.89	0.12	1.99	4.97	3.77	2.40	0.10	1.13	99.84
GÜR19	64.23	0.38	17.24	4.58	0.11	1.56	5.14	3.72	1.96	0.12	0.70	99.74
GÜR20*	64.10	0.42	16.38	4.47	0.12	1.70	4.96	3.70	1.97	0.13	1.13	99.08
EGR23	66.72	0.53	15.62	4.03	0.09	1.35	3.51	3.52	3.53	0.15	0.70	99.75
EGR24*	69.73	0.36	14.57	2.68	0.06	0.82	2.29	4.06	3.97	0.10	0.77	99.41
EGR27*	67.84	0.45	15.18	3.17	0.07	1.03	2.94	3.45	3.89	0.12	1.06	99.19

*Retrieved from Altunkaynak et al. (2012a, 2012b).

a result of the presence of natural building materials in dwellings. A standard room model describes the environment indoors and has to be considered for radioactive dose calculations. According to previous studies (Krisiuk et al., 1971; Stranden, 1979; Koblinger, 1984), the following typical room models are widely acknowledged: 1) a room with 4 × 5 × 2.8 m dimensions, having walls 2350 kg m^{-3} dense and 0.2 m thick; 2) a shell of spherical shape with 2.7 m radius, 0.223 m peripheral thickness, and 1890 kg m^{-3} dense; 3) a hole with an infinitely thick medium around it. The indices introduced by the European Commission (1999), as well as the first room model (parallelepiped) having no doors and windows, have been used in our study. Considering that construction materials should cause external exposure of less than 1 mSv $year^{-1}$, the external gamma index (I_γ) is calculated as followed:

$$I_\gamma = \frac{C_{Ra}}{300} + \frac{C_{Th}}{200} + \frac{C_K}{3000} \quad (1)$$

C_{Ra}, C_{Th}, and C_K represent the activities of ^{226}Ra, ^{232}Th, and ^{40}K (Bq kg^{-1}), respectively. The annual effective doses would be increased by <0.3 mSv per year when samples have $I_\gamma < 2$. Samples with $2 < I_\gamma < 6$ would cause an increment to the effective dose by 1 mSv per year. In the event that the excess of gamma-radiation due to building materials used in small volumes (tiles, boards, etc.) increases the annual effective dose by a maximum of 0.3 mSv, the building

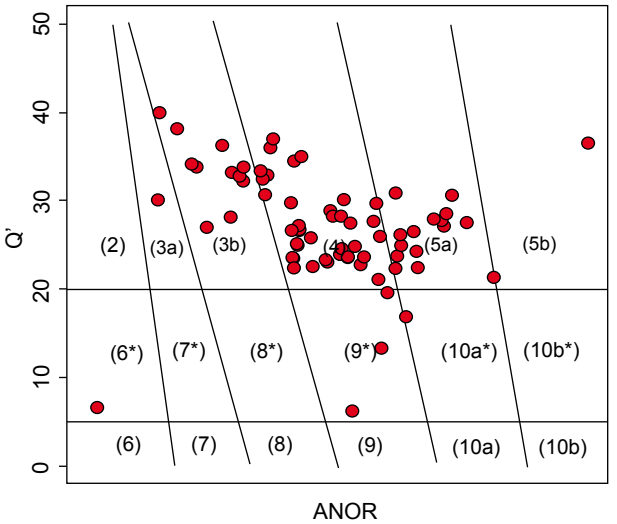

Figure 4. Classification of the samples according to Q'ANOR diagram (Streckeisen and Le Maitre, 1979) (2- Alkali-feldspar granite, 3a- syenogranite, 3b- monzogranite, 4- granodiorite, 5a- tonalite, 5b- calcic tonalite, 6*- alkali-feldspar quartz-syenite, 7*- quartz syenite, 8*- quartz monzonite, 9*- quartz monzodiorite, 10a*- quartz diorite, 10b*- quartz gabbro, 6- alkali-feldspar syenite, 7- syenite, 8- monzonite, 9- monzogabbro, 10a- diorite, 10b- gabbro).

materials should be exempted from all restrictions concerning radioactivity. On the contrary, dose rates of >1 mSv year^{-1} are permitted in exceptional cases and the materials should only locally be used. Consequently, the use of samples with $I_\gamma > 6$ should be restricted (European Commission, 1999).

The EU and ICRP consider 200 Bq m^{-3} as the action level for radon exposure indoors (European Commission, 1990; ICRP, 1994; Righi and Bruzzi, 2006). Assuming that a building material with ^{226}Ra concentration of <200 Bq kg^{-1} could not cause radon concentration of >200 Bq m^{-3} indoors, the following formula has been used to calculate internal α-radiation exposure:

$$I_\alpha = \frac{C_{Ra}}{200} \le 1 \quad (2)$$

C_{Ra} is the specific activity of ^{226}Ra (Bq kg^{-1}). The external radiation index (I_γ) is roughly two times the internal (I_α) (Figure 6). Excepting samples CAT2 and ORH6, the I_γ values of all the samples studied are ≤2 (see Table 6), while I_α values are <1 with the exception of sample CAT2. Therefore, the recommendations for external and internal radiation are fulfilled for 97% of the samples. Only 3% of the samples should be used at local levels and in exceptional cases.

The calculated radioactive indices refer to a standard room with massive granite walls. In order to estimate the actual dose received per year in a more realistic way, the application of granite as tiles 1.5 cm thick instead of massive walls, covering only the floor, should be considered (Anjos et al., 2005, 2011; Mao et al., 2006; Salas et al., 2006). The absorbed gamma dose rate (D_a, nGy h^{-1}) would then be calculated as:

$$D_a(nGy \cdot h^{-1}) = 0.172 \cdot C_{Ra} + 0.217 \cdot C_{Th} + 0.015 \cdot C_K \quad (3)$$

where C_{Ra}, C_{Th}, and C_K represent the activity concentrations (Bq kg^{-1}) of ^{226}Ra, ^{232}Th, and ^{40}K in the samples. Then, considering an indoor occupancy factor T of 7000 h per year (implying that 80% of the annual time is spent inside the standard room model) and a conversion factor F = 0.7 Sv Gy^{-1}, the increase of the effective dose rate due to γ-radiation received indoors can be calculated as:

$$H_{ext}(mSv.y^{-1}) = 10^{-6} \cdot (0.7 \cdot D_a \cdot 7000) \quad (4)$$

The effective dose rate due to radon exposure inside the standard room is calculated as:

$$H_{\text{int}}(mSv.y^{-1}) = 10^{-3} \cdot (f_{P-eq} \cdot D_c \cdot B \cdot F \cdot C_{Rn}) \quad (5)$$

where C_{Rn} is the Rn concentration indoors (Bq m^{-3}), F is the equilibrium factor between Rn and its decay products, $f_{p\text{-}eq}$ is the conversion factor from the equilibrium equivalent Rn concentration ($F \cdot C_{Rn}$) to potential α-energy concentration (5.56×10^{-9} J m^{-3} per Bq m^{-3}), D_c is the conversion factor from potential α-energy concentration to the effective dose (2 Sv/J), and B is the annual breathing rate (7013 m^3 year^{-1}). For a well-ventilated room the equilibrium factor F varies from 0.5 to 0.7, and therefore Eq. (5) gives 1 Bq m^{-3} of Rn corresponding to an effective dose rate due to α-particles varying from 0.039 to 0.055 mSv year^{-1} (European Union, 1990; ICRU, 1994).

The radon concentrations in the case that the floor of the room is covered by granite can be determined as:

$$C_{Rn}(Bq.m^{-3}) = \frac{(1/2) \cdot C_{Ra} \cdot \varepsilon \cdot \lambda \cdot \rho \cdot d \cdot S}{V \cdot (\lambda_v + \lambda)} \quad (6)$$

Considering the parallelepiped standard room with ventilation rate λ_v = 1 h^{-1} (that corresponds to an equilibrium factor F = 0.7) and the floor covered by granite tiles with 1.5 cm thickness (d), 2650 kg m^{-3} density (ρ), and 8% emanation factor (ε) as representative values, the internal effective dose rate is calculated as (Bruzzi et al., 1992; Stoulos et al., 2003; Anjos et al., 2011):

$$H_{\text{int}}(mSv.y^{-1}) = 0.0026 \cdot C_{Ra} \quad (7)$$

Considering good ventilation indoors, the increase of both the external and internal dose received annually caused by the application of the Western Anatolian

Table 3. Rock type, grain size, colour, and mineralogical composition of the samples.

Sample	Rock type	Grain size (mm)	Colour	Modal mineralogy
AS209	bi-hb bt	4–5	Pinkish	Quartz, K-feldspars, plagioclase, hornblende, biotite, zircon, apatite, epidote, titanite, opaques
AS211	bi-hb gd	4	Grey	Quartz, K-feldspars, plagioclase, hornblende, biotite, zircon, chlorite, epidote, titanite, opaques
AS234	bi-hb gd	4	Grey	Quartz, K-feldspars, plagioclase, hornblende, biotite, muscovite, zircon, apatite, chlorite, allanite, titanite, opaques
AS236	bi-hb gt	3	Dark grey	Quartz, K-feldspars, plagioclase, hornblende, biotite, zircon, apatite, chlorite, allanite, titanite, opaques
AS238	bi-hb gd	3	Grey	Quartz, K-feldspars, plagioclase, hornblende, biotite, chlorite, epidote, titanite, opaques
AS239	bi-hb gd	4–5	Grey	Quartz, K-feldspars, plagioclase, hornblende, biotite, zircon, apatite, chlorite, allanite, opaques
AS240	bi-hb gd	3–4	Grey	Quartz, K-feldspars, plagioclase, hornblende, biotite, chlorite, allanite, epidote, titanite, opaques
AS241	bi-hb gd	2–3	Dark grey	Quartz, K-feldspars, plagioclase, hornblende, biotite, zircon, apatite, chlorite, titanite, opaques
AS245	bi-hb gd	3–4	Grey	Quartz, K-feldspars, plagioclase, hornblende, biotite, zircon, apatite, chlorite, titanite, opaques
AS248	bi-hb gd	4	Grey	Quartz, K-feldspars, plagioclase, hornblende, biotite, zircon, apatite, chlorite, epidote, opaques
ÇAT1	bi gt	2–3	White	Quartz, K-feldspars, plagioclase, biotite, zircon, apatite, chlorite, allanite, epidote, titanite, opaques
ÇAT2	gt	1–2	Grey	Quartz, K-feldspars, plagioclase, biotite, muscovite, zircon, garnet, opaques
ÇAT3	bi gt	3–4	Grey	Quartz, K-feldspars, plagioclase, biotite, zircon, apatite, chlorite, allanite, epidote, titanite, opaques
ÇAT4	bi gd	4–5	Grey	Quartz, K-feldspars, plagioclase, biotite, muscovite, zircon, apatite, chlorite, allanite, opaques
ÇAT5	Afdsgt	2	White	Quartz, K-feldspars, plagioclase, biotite, muscovite, zircon, garnet, opaques
ÇAT6	Afdsgt	2	Grey	Quartz, K-feldspars, plagioclase, biotite, muscovite, zircon, garnet, opaques
OS388	bi gt	2–3	Grey	Quartz, K-feldspars, plagioclase, biotite, muscovite, zircon, chlorite, monazite, opaques
OS409	two mica Afdsgt	2–3	Grey	Quartz, K-feldspars, plagioclase, biotite, muscovite, zircon, chlorite, opaques
ULU3	bi gt	3–4	Grey	Quartz, K-feldspars, plagioclase, biotite, muscovite, zircon, apatite, opaques
ULU5	bi gt	4	Grey	Quartz, K-feldspars, plagioclase, biotite, muscovite, apatite, opaques
ULU6	bi gt	3	Grey	Quartz, K-feldspars, plagioclase, biotite, muscovite, chlorite, opaques

Table 3. (Continued).

ULU8	bi gt	2–3	Grey	Quartz, K-feldspars, plagioclase, biotite, muscovite, zircon, garnet, opaques
ULU11	bi gt	3–4	Grey	Quartz, K-feldspars, plagioclase, biotite, muscovite, zircon, chlorite, opaques
ULU12	two mica gt	4	Grey	Quartz, K-feldspars, plagioclase, biotite, muscovite, zircon, chlorite, opaques
EYB10	bi-hb Qz diorite	3–4	Dark grey	Quartz, K-feldspars, plagioclase, hornblende, biotite, zircon, apatite, epidote, titanite, opaques
EYB14	hb ton	3	Dark grey	Quartz, K-feldspars, plagioclase, hornblende, zircon, apatite, chlorite, allanite, epidote, titanite, opaques
EYB15	bi-hb ton	4	Dark grey	Quartz, K-feldspars, plagioclase, hornblende, biotite, zircon, apatite, chlorite, allanite, titanite, opaques
EYB24	hb Qz diorite	4–5	Grey	Quartz, K-feldspars, plagioclase, hornblende, biotite, zircon, allanite, titanite, opaques
EYB30	hb Qz diorite	4–5	Dark grey	Quartz, K-feldspars, plagioclase, hornblende, biotite, chlorite, epidote, titanite, opaques
EYB34	bi-hb ton	3–4	Grey	Quartz, K-feldspars, plagioclase, hornblende, biotite, zircon, apatite, chlorite, titanite, opaques
EYB35	hb gd	4	Grey	Quartz, K-feldspars, plagioclase, hornblende, biotite, zircon, apatite, chlorite, titanite, opaques
EYB38	hb ton	3	Grey	Quartz, K-feldspars, plagioclase, hornblende, biotite, zircon, apatite, chlorite, allanite, titanite, opaques
KOZ1	bi gt	2–3	Grey	Quartz, K-feldspars, plagioclase, hornblende, biotite, zircon, apatite, allanite, opaques
KOZ2	hb-bi gt	4–5	Grey	Quartz, K-feldspars, plagioclase, hornblende, biotite, zircon, chlorite, titanite, opaques
KOZ4	hb bi gt	3–4	Grey	Quartz, K-feldspars, plagioclase, hornblende, biotite, zircon, epidote, opaques
KOZ5	bi gt	2	Grey	Quartz, K-feldspars, plagioclase, hornblende, biotite, zircon, chlorite, opaques
KOZ8	bi gt	3	Grey	Quartz, K-feldspars, plagioclase, biotite, zircon, apatite, chlorite, allanite, opaques
KOZ9	bi gt	2–3	Dark grey	Quartz, K-feldspars, plagioclase, hornblende, biotite, zircon, chlorite, opaques
KOZ10	hb bi gt	3–4	Dark grey	Quartz, K-feldspars, plagioclase, hornblende, biotite, zircon, chlorite, allanite, titanite, opaques
EVC1	bi hb gd	3–4	Grey	Quartz, K-feldspars, plagioclase, hornblende, biotite, zircon, apatite, chlorite, epidote, titanite, opaques
EVC2	bi gd	4	Grey	Quartz, K-feldspars, plagioclase, hornblende, biotite, zircon, apatite, chlorite, epidote, titanite, opaques
EVC3	hb gd	3–4	Grey	Quartz, K-feldspars, plagioclase, hornblende, biotite, zircon, apatite, chlorite, allanite, epidote, titanite, opaques
EVC5	bi hb gt	4	Grey	Quartz, K-feldspars, plagioclase, hornblende, biotite, zircon, chlorite, allanite, titanite, opaques

Table 3. (Continued).

EVC6	bi gd	4–5	Grey	Quartz, K-feldspars, plagioclase, hornblende, biotite, zircon, chlorite, titanite, opaques
EVC8	hb bi ton	4	Grey	Quartz, K-feldspars, plagioclase, hornblende, biotite, apatite, chlorite, titanite, opaques
ORH1	bi hb ton	3–4	Dark grey	Quartz, K-feldspars, plagioclase, hornblende, biotite, zircon, apatite, chlorite, titanite, opaques
ORH3	bi hb ton	5	Grey	Quartz, K-feldspars, plagioclase, hornblende, biotite, zircon, apatite, chlorite, titanite, opaques
ORH5	bi hb ton	2	Grey	Quartz, K-feldspars, plagioclase, hornblende, biotite, zircon, chlorite, epidote, opaques
ORH6	hb qz syenite	3–4	Pinkish	Quartz, K-feldspars, plagioclase, hornblende, biotite, clinopyroxene, zircon, allanite, epidote, titanite, opaques
KAP42	bi gt	3–4	Grey	Quartz, K-feldspars, plagioclase, biotite, zircon, apatite, chlorite, epidote, opaques
KAP43	hb bi gt	2–3	Dark grey	Quartz, K-feldspars, plagioclase, hornblende, biotite, zircon, apatite, chlorite, epidote, opaques
KAP45	hb bi ton	3–4	Dark grey	Quartz, K-feldspars, plagioclase, hornblende, biotite, zircon, apatite, chlorite, epidote, opaques
KAP46	gt	3	Grey	Quartz, K-feldspars, plagioclase, biotite, muscovite, zircon, epidote, opaques
KAP47	bi hb ton	1–2	Dark grey	Quartz, K-feldspars, plagioclase, hornblende, biotite, zircon, apatite, chlorite, epidote, opaques
KAP52	bi gd	3	Grey	Quartz, K-feldspars, plagioclase, hornblende, biotite, chlorite, titanite, opaques
CAM28	bi gt	4-5	Grey	Quartz, K-feldspars, plagioclase, biotite, chlorite, epidote, opaques
CAM29	bi gt	4–5	Grey	Quartz, K-feldspars, plagioclase, biotite, zircon, apatite, chlorite, allanite, opaques
CAM30	bi hb gd	3	Grey	Quartz, K-feldspars, plagioclase, hornblende, biotite, zircon, apatite, chlorite, titanite, opaques
TOP9	bi hb gd	4	Grey	Quartz, K-feldspars, plagioclase, hornblende, biotite, zircon, apatite, chlorite, epidote, opaques
TOP11	bi hb gd	2	Dark grey	Quartz, K-feldspars, plagioclase, hornblende, biotite, clinopyroxene, zircon, apatite, chlorite, epidote, opaques
TOP12	bi hb gd	4	Grey	Quartz, K-feldspars, plagioclase, hornblende, biotite, zircon, apatite, chlorite, opaques
TPL1	bi hb dior	3	Grey	Quartz, K-feldspars, plagioclase, hornblende, biotite, chlorite, epidote, opaques
TPL13	bi hbgt	5	Grey	Quartz, K-feldspars, plagioclase, hornblende, biotite, zircon, apatite, chlorite, opaques
TPL14	bi hb Qz diorite	4	Dark grey	Quartz, K-feldspars, plagioclase, hornblende, biotite, zircon, apatite, chlorite, epidote, titanite, opaques
GÜR18	bi hb gd	4	Grey	Quartz, K-feldspars, plagioclase, hornblende, biotite, zircon, apatite, chlorite, titanite, opaques

Table 3. (Continued).

GÜR19	bi hb gd	4	Grey	Quartz, K-feldspars, plagioclase, hornblende, biotite, zircon, apatite, chlorite, titanite, opaques
GÜR20	bi hb gd	4	Grey	Quartz, K-feldspars, plagioclase, hornblende, biotite, zircon, apatite, chlorite, opaques
EGR23	hb bi gt	4	Grey	Quartz, K-feldspars, plagioclase, hornblende, biotite, zircon, apatite, chlorite, epidote, opaques
EGR24	hb bi gt	4	Grey	Quartz, K-feldspars, plagioclase, hornblende, biotite, zircon, apatite, epidote, titanite, opaques
EGR27	hb bi gt	4	Pinkish	Quartz, K-feldspars, plagioclase, hornblende, biotite, zircon, apatite, chlorite, opaques

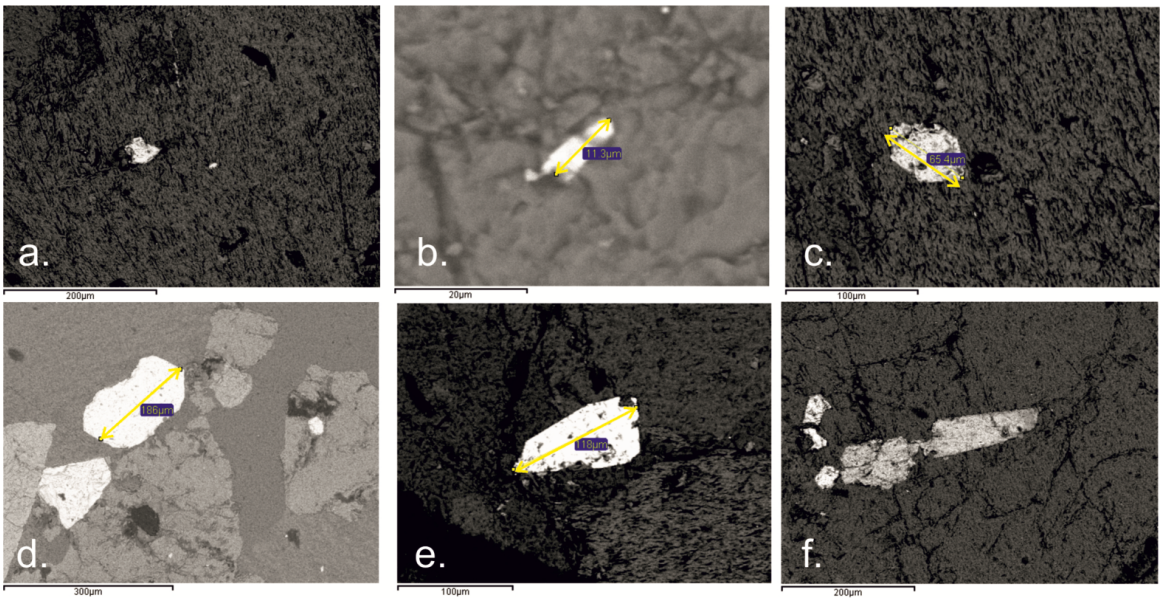

Figure 5. Backscattered electron images of selected grains of accessory minerals. a) Monazite from sample OS388, b) zircon from sample CAT2, c) zircon from sample OS388, d) zircon from sample ORH6, e) zircon from sample OS388, f) allanite from sample CAT1.

Table 4. Pearson correlation coefficients of selected radionuclides and K_2O/SiO_2.

		^{226}Ra	^{232}Th	^{40}K	K_2O/SiO_2
^{226}Ra	Pearson correlation	1	0.558**	–0.383**	0.382**
	Sig. (2-tailed)		0.000	0.001	0.001
^{232}Th	Pearson correlation	0.558**	1	–0.512**	0.385**
	Sig. (2-tailed)	0.000		0.000	0.001
^{40}K	Pearson correlation	–0.383**	–0.512**	1	–0.338**
	Sig. (2-tailed)	0.001	0.000		0.004
K_2O/SiO_2	Pearson correlation	0.382**	0.385**	–0.338**	1
	Sig. (2-tailed)	0.001	0.001	0.004	

*Correlation is significant at the 0.05 level (2-tailed).
**Correlation is significant at the 0.01 level (2-tailed).
Number of samples = 70.

Table 5. Activities (Bq kg^{-1}) of ^{226}Ra, ^{232}Th, and ^{40}K in various granite samples worldwide. Mean value ± standard error* (min–max).

	^{226}Ra	^{232}Th	^{40}K	
Turkey	58 ± 5	90 ± 5	1097 ± 48	
Raw samples (70)	(11–230)	(0.1–241)	(148–2518)	This work
Turkey	92 ± 7	98 ± 10	1155 ± 103	
Imported samples (30)	(0.7–186)	(0.5–249)	(0.4–1935)	Cetin et al., 2012
Imported samples (42)	(9–193)	(7–345)	(92–4156)	Turhan, 2012
Greece	74 ± 5	85 ± 5	881 ± 30	
Raw samples (121)	(1–315)	(2–376)	(55–1632)	Papadopoulos et al., 2013
Greece	64 ± 13	81 ± 20	1104 ± 102	
Imported samples (16)	(1–170)	(<354)	(49–1592)	Pavlidou et al., 2006
Cyprus	77 ± 22	143 ± 34	1215 ± 67	
Imported samples (28)	(1–588)	(<906)	(50–1606)	Tzortzis et al., 2003
Egypt	138 ± 17	82 ± 12	1081 ± 110	
Imported samples (27)	(25–356)	(5–161)	(100–1796)	Amin, 2012
Japan	43 ± 5	72 ± 7	1004 ± 36	
Commercial samples (40) Imported samples (49)	(5–120) (4–250)	(5–250) (2–300)	(130–1500) (70–1800)	Iwaoka et al., 2013
Italy	112 ± 27	107 ± 27	1063 ± 105	
Commercial samples (20)	(12–390)	(20–490)	(240–2000)	Marocchi et al., 2011
USA	31 ± 6	61 ± 6	1210 ± 33	
Commercial samples (22)	(6–130)	(7 – 150)	(120–1900)	Kitto et al., 2009
Brazil	45 ± 19	106 ± 48	1320 ± 170	
Commercial samples (300)	(5–160)	(4 – 450)	(190–2029)	Anjos et al., 2005, 2011
Commercial samples (100)	(<600)	(<530)	(<2300)	Salas et al., 2006
Commercial samples (14)	(10–252)	(9–347)	(407–1435)	Moura et al., 2011
China	90 ± 11	94 ± 14	1060 ± 121	
Commercial samples (76)	(3–762)	(3 – 358)	(62–1539)	Mao et al., 2006
Commercial samples (81)	(4–347)	(1 – 276)	(17–3357)	Xinwei et al., 2006
Worldwide	78	111		
	(1–370)	(1–1030)		UNSCEAR, 1993

* $St.Error = St..Deviation \sqrt{No_{samples}}$

granites as construction material is given in Figure 7. The shape of the distribution of frequency of the external γ-radiation effective dose rate is Gaussian (Kolmogorov–Smirnov test, P-value = 0.48), and its mean value was 0.21 (±0.09) mSv year^{-1}, varying by <0.5 mSv year^{-1}. According to the European Commission (1999), all the samples but one (CAT2) could be used in construction, as the increment in the effective γ-dose is <1 mSv year^{-1}. As far as the internal α-radiation is concerned, it is normally distributed (Kolmogorov–Smirnov test, P-value = 0.25) and has a mean value of 0.15 (±0.10) mSv year^{-1} varying by <0.60 mSv year^{-1}. The increase in external effective dose rate is greater than that of the internal effective dose rate. Considering a well-ventilated room, the average increase for the inhabitants in the internal radiation caused by radon exposure by the samples studied is 9.4 % of the maximum permitted value of 1.6 mSv year^{-1}. All samples but AS211 and AS238 from the Ilıca pluton; CAT1, CAT2, CAT5, and OS388 from the Çataldağ pluton; and ORH6 from the Orhaneli pluton increase the internal dose by <30% of the limit.

The increase in total effective dose rate (H_{ext} + H_{int}, hereafter H_{tot}) caused by the application of Western Anatolian granites in the case that they only cover the

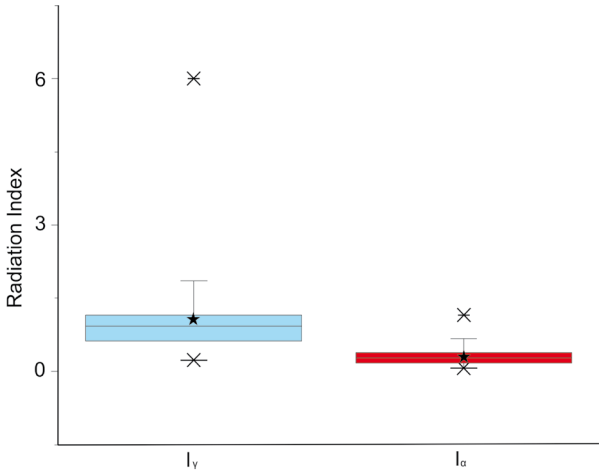

Figure 6. Variations of external (I_γ) and internal (I_α) indices of the Western Anatolian granites. The box corresponds to the standard error while the whisker corresponds to the standard deviation. The black stars correspond to the average while the line within the box corresponds to the median.

floor of the room varies from 0.00 to 1.06 mSv year^{-1} with a mean value of 0.31 (±0.21) mSv year^{-1}. According to the location of each sample, these are displayed in Figure 8. Samples from the Çataldağ pluton show the highest average activities of radionuclides and thus values of radioactive indices.

Aiming to make comparisons between the excess of the H_{tot} due to the Western Anatolian samples and samples from other places of origin, the data of Table 5 have been used in Eqs. (4) and (7). Western Anatolian samples present lower excess H_{tot} relative to the granites imported in Turkey and one of the lowest among the imported granites in the SE Mediterranean countries. The average increase of H_{tot} of the two major exporters worldwide, Brazil and China, is calculated as 0.36 and 0.49 mSv year^{-1}, respectively, being similar to that of the Western Anatolian granite samples.

PCA is the most common technique used to summarise large datasets. Varimax rotation with the Kaiser normalisation method was used for the evaluation

Table 6. Radioactivity indices calculated for Western Anatolian granites: external gamma index (I_γ), internal alpha index (I_α), and the increment of the gamma (H_{ext}) and alpha (H_{int}) effective dose rates (mSv year^{-1}).

		I_γ	I_α	H_{ext}	H_{int}
AS209	Ilıca	1.33	0.38	0.30	0.20
AS211	Ilıca	1.67	0.40	0.37	0.21
AS234	Ilıca	1.08	0.17	0.24	0.09
AS236	Ilıca	0.65	0.46	0.15	0.24
AS238	Ilıca	1.49	0.44	0.33	0.23
AS239	Ilıca	1.14	0.27	0.25	0.14
AS240	Ilıca	1.00	0.30	0.22	0.16
AS241	Ilıca	1.37	0.50	0.31	0.26
AS245	Ilıca	0.98	0.21	0.22	0.11
AS248	Ilıca	0.86	0.23	0.19	0.12
ÇAT1	Çataldağ	1.38	0.67	0.31	0.35
ÇAT2	Çataldağ	2.03	1.15	0.47	0.60
ÇAT3	Çataldağ	1.24	0.41	0.28	0.21
ÇAT4	Çataldağ	1.44	0.48	0.32	0.25
ÇAT5	Çataldağ	0.89	0.2	0.20	0.10
ÇAT6	Çataldağ	0.56	0.27	0.13	0.14
OS388	Çataldağ	1.85	0.78	0.42	0.41
OS409	Çataldağ	1.14	0.37	0.26	0.19
ULU3	Uludağ	0.84	0.29	0.19	0.15
ULU5	Uludağ	1.10	0.36	0.25	0.19
ULU6	Uludağ	1.13	0.33	0.25	0.17
ULU8	Uludağ	0.97	0.46	0.22	0.24
ULU11	Uludağ	1.02	0.46	0.23	0.24
ULU12	Uludağ	0.90	0.35	0.20	0.18

Table 6. (Continued).

EYB10	Eybek	0.55	0.16	0.12	0.08
EYB14	Eybek	0.65	0.21	0.15	0.11
EYB15	Eybek	0.67	0.18	0.15	0.10
EYB24	Eybek	-	-	-	-
EYB30	Eybek	0.52	0.17	0.12	0.09
EYB34	Eybek	0.73	0.17	0.16	0.09
EYB35	Eybek	0.6	0.14	0.13	0.07
EYB38	Eybek	0.74	0.21	0.16	0.11
KOZ1	Kozak	1.06	0.27	0.24	0.14
KOZ2	Kozak	1.02	0.24	0.23	0.13
KOZ4	Kozak	1.02	0.3	0.23	0.16
KOZ5	Kozak	1.25	0.43	0.28	0.22
KOZ8	Kozak	1.35	0.29	0.30	0.15
KOZ9	Kozak	1.17	0.26	0.26	0.14
KOZ10	Kozak	-	-	-	-
EVC1	Evciler	-	-	-	-
EVC2	Evciler	1.02	0.21	0.23	0.11
EVC3	Evciler	1.01	0.3	0.23	0.15
EVC5	Evciler	1.14	0.42	0.26	0.22
EVC6	Evciler	-	-	-	-
EVC8	Evciler	-	-	-	-
ORH1	Orhaneli	0.44	0.08	0.10	0.04
ORH3	Orhaneli	0.45	0.08	0.10	0.04
ORH5	Orhaneli	0.45	0.08	0.10	0.04
ORH6	Orhaneli	2.27	0.58	0.51	0.30
KAP42	Kapıdağ	0.64	0.08	0.14	0.04
KAP43	Kapıdağ	0.82	0.21	0.18	0.11
KAP45	Kapıdağ	0.62	0.09	0.14	0.05
KAP46	Kapıdağ	0.24	0.06	0.05	0.03
KAP47	Kapıdağ	0.55	0.10	0.12	0.05
KAP52	Kapıdağ	0.62	0.31	0.14	0.16
CAM28	Çamlık	-	-	-	-
CAM29	Çamlık	-	-	-	-
CAM30	Çamlık	0.93	0.33	0.21	0.17
TOP9	Topuk	0.84	0.28	0.19	0.15
TOP11	Topuk	-	-	-	-
TOP12	Topuk	0.69	0.09	0.15	0.05
TPL1	Tepeldağ	-	-	-	-
TPL13	Tepeldağ	0.91	0.11	0.20	0.06
TPL14	Tepeldağ	0.27	0.06	0.06	0.03
GÜR18	Gürgenyayla	0.46	0.11	0.10	0.06
GÜR19	Gürgenyayla	-	-	-	-
GÜR20	Gürgenyayla	0.49	0.13	0.11	0.07
EGR23	Eğrigöz	0.88	0.21	0.20	0.11
EGR24	Eğrigöz	0.95	0.25	0.21	0.13
EGR27	Eğrigöz	1.08	0.17	0.24	0.09

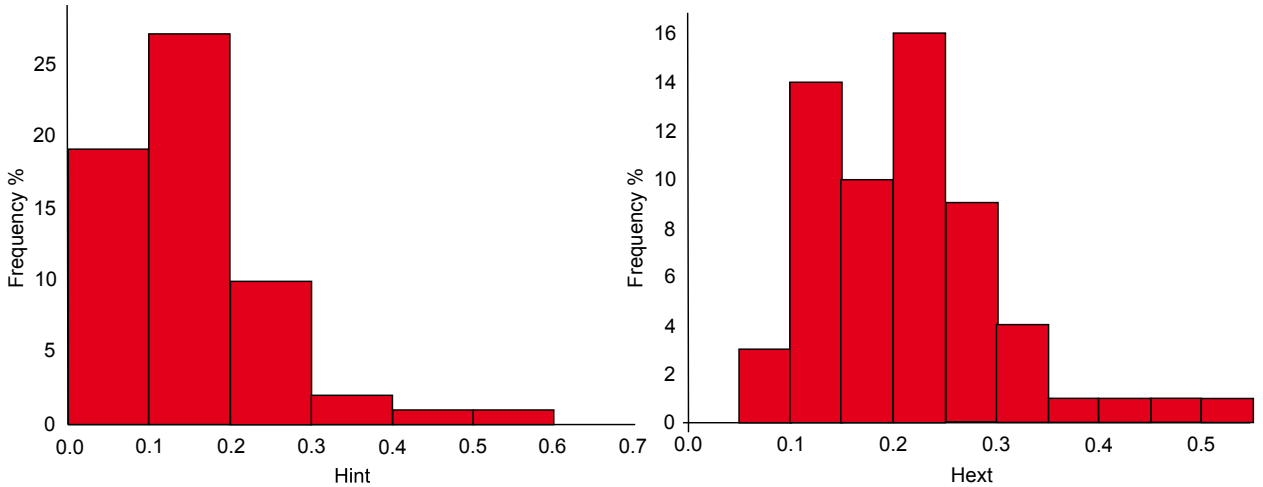

Figure 7. Annual effective dose (internal and external) (H, mSv year^{-1}) in a well-ventilated indoor environment from the application of the Western Anatolian granites as ornamental stones.

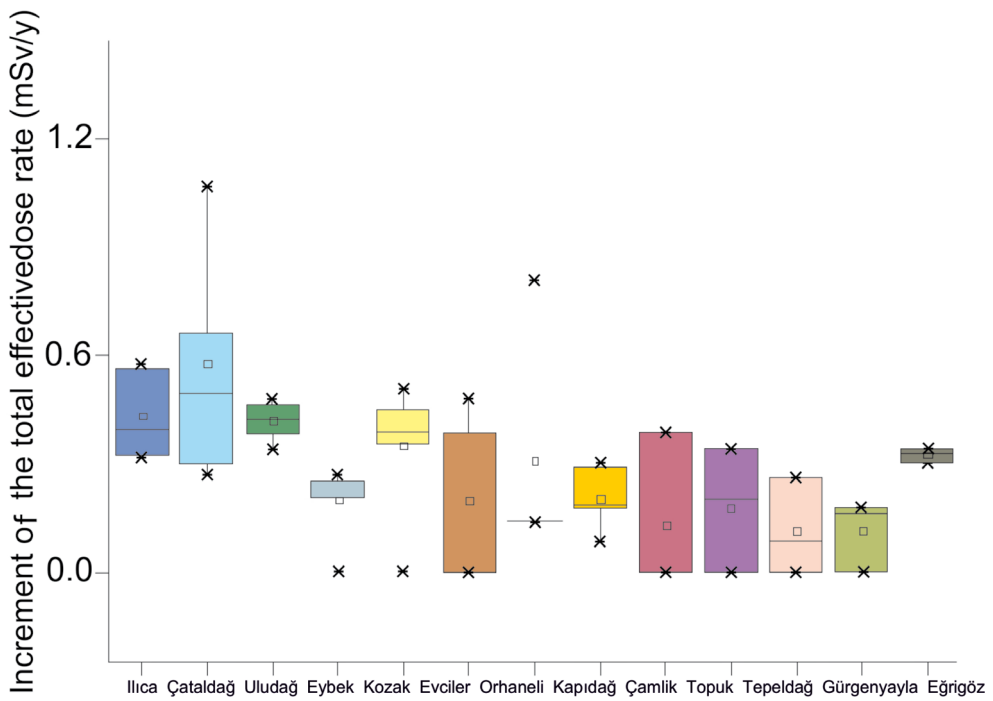

Figure 8. Variations according to the location of the annual effective dose external plus internal (total effective dose) indoors caused by the application of the Western Anatolian granites. The box corresponds to the standard error while the whisker corresponds to the standard deviation. The black stars correspond to the average while the line within the box corresponds to the median. The white stars correspond to values that range beyond the standard deviation.

of PCA. In order to conduct the relevant statistical analysis of the data, SPSS 16.0 was used.

In Table 7, the results of the factor loadings (obtained after a varimax rotation), the eigenvalues, and the communalities are given. According to the results, there were 3 eigenvalues of >1 explaining 77.78% of the total variance, which is good as it is >75% (Zhang et al., 2005). As seen from Tables 7 and 8, the first component (PC1) explained 36.37% of the variance in total and was correlated mainly with major oxides such as SiO_2, Al_2O_3,

Table 7. Principal components, their eigenvalues, and the sums of squared loadings.

Component	Initial eigenvalues			Rotation sums of squared loadings		
	Total	% of variance	Cumulative %	Total	% of variance	Cumulative %
1	8.588	47.713	47.713	6.547	36.371	36.371
2	3.742	20.792	68.505	5.537	30.760	67.131
3	1.670	9.275	77.780	1.917	10.649	77.780
4	0.868	4.824	82.604			
5	0.793	4.403	87.007			
6	0.629	3.494	90.501			
7	0.531	2.952	93.453			
8	0.400	2.222	95.675			
9	0.272	1.509	97.184			
10	0.248	1.380	98.564			
11	0.112	0.623	99.188			
12	0.077	0.427	99.615			
13	0.033	0.182	99.797			
14	0.015	0.084	99.881			
15	0.011	0.059	99.941			
16	0.010	0.057	99.998			
17	0.000	0.001	99.999			
18	0.000	0.001	100.000			

Table 8. Rotated factor loadings of the extracted components.

	Component		
	1	2	3
Rock type	0.044	–0.588	0.266
SiO_2	–0.948	0.166	0.203
Al_2O_3	0.802	–0.248	0.041
Fe_2O_3	0.939	–0.172	–0.203
MgO	0.887	–0.148	–0.339
CaO	0.933	–0.282	–0.091
Na_2O	–0.051	0.101	0.766
K_2O	–0.640	0.406	–0.363
TiO_2	0.899	–0.122	–0.297
P_2O_5	0.498	0.117	–0.736
MnO	0.831	–0.065	0.236
^{232}Th	–0.243	0.811	0.082
^{40}K	0.349	–0.540	0.195
^{226}Ra	–0.052	0.682	–0.262
I_γ	–0.142	0.911	0.076
I_α	–0.204	0.917	0.233
H_{ext}	–0.147	0.915	0.082
H_{int}	–0.200	0.918	0.232

Fe_2O_3, MgO, CaO, TiO_2, MnO, and K_2O. Factor 1 is characterised by positive and negative components. Al_2O_3, Fe_2O_3, MgO, CaO, and TiO_2 have positive values while SiO_2 and K_2O have negative values. Factor 1 is represented by the $(Al_2O_3+Fe_2O_3+MgO+CaO+TiO_2)/(SiO_2+K_2O)$ ratio. This ratio could be interpreted as the effects of fractional crystallisation or crustal contamination. The second component (PC2) loaded heavily on the radionuclides and radioactivity indices, ^{232}Th, ^{226}Ra, I_γ, I_α, H_{ext}, and H_{int}, as well as with the rock type, accounting for 30.76% of the total variance. The third component (PC3) accounted for 10.65% of the total variance. PC3 was strongly correlated positively with Na_2O and negatively with P_2O_5 and thus was characterised by the Na_2O/P_2O_5 ratio. This ratio also suggests the crustal contamination effect.

4. Conclusions

The natural radioactivity of the granites studied varied up to 259 Bq kg^{-1} for ^{226}Ra, up to 241 Bq kg^{-1} for ^{232}Th, and up to 2518 Bq kg^{-1} for ^{40}K, with mean values of 66 (±44), 90 (±47), and 1097 (±410) Bq kg^{-1}, respectively. All of them are below or similar to the mean worldwide values of 78 (^{226}Ra) and 111 (^{232}Th) Bq kg^{-1} in the case of the majority of the samples (80% and 77.1%, respectively).

The increment to both the H_{int} and H_{ext} received per year by the application of granite in the form of tiles of 1.5 cm in thickness is calculated taking into account a standard room model where only the floor of the room is covered by granite. The shape of the distribution of the excess on the H_{ext} dose rate is Gaussian, varying by <0.6 mSv year^{-1}, and has a mean value of 0.21 (±0.09) mSv year^{-1}. Considering the international standards and regulations, all but one of the studied samples (sample CAT2) can be used as building and decorative stones, as the increase in H_{ext} is smaller than 30% of the permitted limit.

H_{int} is normally distributed and has a mean of 0.15 (±0.10) mSv year^{-1}, varying by <0.6 mSv year^{-1}. Considering a well-ventilated room, the excess in the internal radiation due to radon exposure caused by the application of the granites of this study as building and decorative materials is only 9.4% of the maximum permitted effective dose of 1.6 mSv year^{-1}. The increase in the internal as well as the external dose caused by the samples of this study is on average <30% of the limit.

The highest H_{tot} is displayed by samples from the Çataldağ pluton (particularly sample CAT2). The average increase in the H_{tot} of Western Anatolian granites is comparable to that of the PCG. Therefore, there is no radiological risk from the usage of the samples studied as decorative and ornamental building materials.

Acknowledgements

This study was supported by grants from İstanbul Technical University (BAP Projects No: 37883 and 36010), the Scientific and Technological Research Council of Turkey (TÜBİTAK-ÇAYDAG-112Y093), and the Research Committee of Aristotle University of Thessaloniki, which are gratefully acknowledged. The authors are also grateful to Subject Editor Prof Ali Elmas, Editor in Chief Prof Fuat Yavuz, Prof Orhan Karslı, and two anonymous reviewers for their constructive comments that aimed to improve this article.

References

Akay E (2009). Geology and petrology of the Simav Magmatic Complex (NW Anatolia) and its comparison with the Oligo-Miocene granitoids in NW Anatolia: implications on Tertiary tectonic evolution of the region. Int J Earth Sci (Geol Rundsch) 98: 1655-1675.

Aldanmaz E, Pearce J, Thirlwall MF, Mitchell J (2000). Petrogenetic evolution of late Cenozoic, post-collision volcanism in western Anatolia, Turkey. J Volcanol Geoth Res 102: 67-95.

Altunkaynak Ş (2007). Collision-driven slab breakoff magmatism in northwestern Anatolia, Turkey. J Geol 115: 63-82.

Altunkaynak Ş, Dilek Y (2006). Timing and nature of postcollisional volcanism in Western Anatolia and geodynamic implications. In: Dilek Y, Pavlides S, editors. Post-Collisional Tectonics and Magmatism of the Eastern Mediterranean Region. Boulder, CO, USA: Geological Society of America Special Papers, pp. 321-351.

Altunkaynak Ş, Dilek Y (2013). Eocene mafic volcanism in northern Anatolia: its causes and mantle sources in the absence of active subduction. Int Geol Rev 55: 1641-1659.

Altunkaynak S, Dilek, Y, Genç SC, Sunal, G, Gertisser R, Furnes H, Foland KA, Yang J (2012a). Spatial, temporal and geochemical evolution of Oligo–Miocene granitoid magmatism in western Anatolia, Turkey. Gondwana Res 21: 961-986.

Altunkaynak Ş, Genç ŞC (2008). Petrogenesis and time-progressive evolution of the Cenozoic continental volcanism in the Biga Peninsula, NW Anatolia (Turkey). Lithos 102: 316-340.

Altunkaynak S, Rogerw NM, Kelley SP (2010). Causes and effects of geochemical variations in Late Cenozoic volcanism of the Foca volcanic centre, NW Anatolia, Turkey. Int Geol Rev 55: 579-607.

Altunkaynak S, Sunal G, Aldanmaz E, Genç SC, Dilek Y, Furnes H, Foland KA, Yang J, Yıldız M (2012b). Eocene granitic magmatism in NW Anatolia (Turkey) revisited: new implications from comparative zircon SHRIMP U-Pb and 40Ar-39Ar geochronology and isotope geochemistry on magma genesis and emplacement. Lithos 155: 289-309.

Altunkaynak Ş, Yılmaz Y (1998). The Kozak magmatic complex; western Anatolia. J Volcanol Geoth Res 85: 211-231.

Amin RM (2012). Gamma radiation measurements of natural occurring radioactivity samples from commercial Egyptian granites. Envir Earth Sci 67: 771-775.

Angi OS, Yavuz O, Yalçin T, Çiftçi E (2016). Mineralogy-induced radiological aspects with characterization of commercial granites exploited in Turkey. Bull Eng Geol Environ (in press).

Anjos RM, Ayub JJ, Cid AS, Cardoso R, Lacerda T (2011). External gamma-ray dose rate and radon concentration in indoor environments covered with Brazilian granites. J Envir Radioact 102: 1055-1061.

Anjos RM, Veiga R, Soares T, Santos AMA, Aguiar JG, Frasca MHBO, Brage JAP, Uzeda D, Mangia L, Facure A et al. (2005). Natural radionuclide distribution in Brazilian commercial granites. Rad Meas 39: 245-253.

Boztuğ D, Harlavan Y, Jonckheere R, Can I, Sarı R (2009). Geochemistry and K-Ar cooling ages of the Ilıca, Çataldağ (Balıkesir) and Kozak (İzmir) granitoids, west Anatolia, Turkey. Geol J 44: 79-103.

Bruzzi L, Mele R, Padoani F (1992). Evaluation of gamma and alpha doses due to natural radioactivity of building materials. J Radiol Prot 12: 67-76.

Cetin E, Altinsoy N, Orgun Y (2012). Natural radioactivity levels of granites used in Turkey. Rad Prot Dosim 151: 299-305.

Cutshall NH, Larsen IL, Olsen CR (1983). Direct analysis of 210Pb in sediment samples: self-absorption corrections. Nucl Instrum Methods B 206: 309-312.

Debertin K, Helmer RG (1988). Gamma- and X-Ray Spectrometry with Semiconductor Detectors. Amsterdam, the Netherlands: North-Holland.

Dilek Y, Altunkaynak Ş (2007). Cenozoic crustal evolution and mantle dynamics of post-collisional magmatism in western Anatolia. Int Geol Rev 49: 431-453.

Dilek Y, Altunkaynak Ş (2010). Geochemistry of Neogene-Quaternary alkaline volcanism in western Anatolia, Turkey, and implications for the Aegean mantle. Int Geol Rev 52: 631-655.

Erkül F (2010). Tectonic significance of synextensional ductile shear zones within the Early Miocene Alaçamdağ granites, northwestern Turkey. Geol Mag 147: 611-637.

Erkül F, Erkül ST, Ersoy Y, Uysal İ, Klötzli U (21013). Petrology, mineral chemistry and Sr-Nd-Pb isotopic compositions of granitoids in the central Menderes Core Complex: constraints on the evolution of Aegean lithosphere slab. Lithos 180-181: 74-91.

Erkül ST (2012). Petrogenetic evolution of the Early Miocene Alaçamdağ volcano-plutonic complex, northwestern Turkey: implications for the geodynamic framework of the Aegean region. Int J Earth Sci 101: 197-219.

Erkül ST, Erkül F (2012). Magma interaction processes in syn-extensional granitoids: the Tertiary Menderes Metamorphic Core Complex, western Turkey. Lithos 142-143: 16-33.

Erkül ST, Özmen SF, Erkül F, Boztosun I (2016). Comparison between natural radioactivity levels and geochemistry of some granitoids in western Turkey. Turkish J Earth Sci 25: 242-255.

Ersoy YE, Helvacı C, Palmer MR (2009). Petrogenesis of the Neogene volcanic units in the NE-SW-trending basins in western Anatolia, Turkey. Contrib Mineral Petrol 163: 379-401.

European Commission (1999). Radiation Protection 112: Radiological Protection Principles Concerning the Natural Radioactivity of Building Materials. Brussels, Belgium: Directorate – General Environment, Nuclear Safety and Civil Protection.

Genç C (1998). Evolution of the Bayramiç magmatic complex, northwestern Anatolia. J Volcanol Geoth Res 85: 233-249.

Gilmore G (2008). Practical Gamma-Ray Spectrometry. 2nd ed. New York, NY, USA: John Wiley & Sons.

Güleç N (1991). Crust-mantle interaction in western Turkey: implications from Sr and Nd isotope geochemistry of Tertiary and Quaternary volcanics. Geol Mag 23: 417-435.

Harris NBW, Kelley S, Okay AI (1994). Post-collisional magmatism and tectonics in northwest Anatolia. Contrib Mineral Petrol 117: 241-252.

Hasözbek A, Satır M, Erdoğan B, Akay E, Siebel W (2010). Early Miocene post-collisional magmatism in NW Turkey: geochemical and geochronological constraints. Int Geol Rev 53: 1098-1119.

Iwaoka K, Hosoda M, Tabe H, Iishikawa T, Tokonami S, Yonehara H (2013). Activity concentration of natural radionuclides and radon and thoron exhalation rates in rocks used as decorative wall coverings in Japan. Health Phys 104: 41-50.

Karadeniz O, Akal C (2014). Radiological mapping in the granodiorite area of Bergama (Pergamon)-Kozak, Turkey. J Radioanal Nucl Chem 302: 361-373.

Karadeniz Ö, Çıyrak N, Yaprak G, Akal C (2011). Terrestrial gamma exposure in the granodiorite area of Bergama (Pergamon)-Kozak, Turkey. J Radianal Nucl Chem 302: 361-373.

Kitto ME, Haines DK, Menia TA (2009). Assessment of gamma-ray emissions from natural and manmade decorative stones. J. Radioanal Nucl Chem 282: 409-413.

Koblinger L (1984). Mathematical models of external gamma radiation and congruence of measurements. Radiat Prot Dosim 7: 227-234.

Köprübaşı N, Aldanmaz E (2004). Geochemical constraints on the petrogenesis of Cenozoic I-type granitoids in Northwest Anatolia, Turkey: evidence for magma generation by lithospheric delamination in a post-collisional setting. Int Geol Rev 46: 705-729.

Krisiuk EM, Tarasov SI, Shamov VP, Shalak NI, Lisachenko EP, Gomelsky LG (1971). A Study of Radioactivity in Building Materials. Leningrad, USSR: Research Institute for Radiation Hygiene.

Mao Y, Liu Y, Fu Y, Lin L (2006). Physical models and limits of radionuclides for decorative building materials. Health Phys 90: 471-476.

Marocchi M, Righi S, Bargossi GM, Gasprotto G (2011). Natural radionuclides content and radiological hazard of commercial ornamental stones: an integrated radiometric and mineralogical-petrographic study. Rad Meas 46: 538-545.

Moura CL, Artur AC, Bonoto DM, Guedes S, Martinelli CD (2011). Natural radioactivity and radon exhalation rate in Brazilian igneous rocks. Appl Rad Isot 69: 1094-1099.

Okay AI, Satır M (2000). Coeval plutonism and metamorphism in a latest Oligocene metamorphic core complex in northwest Turkey. Geol Mag 137: 495-516.

Okay AI, Satır M (2006). Geochronology of Eocene plutonism and metamorphism in northwest Turkey: evidence for a possible magmatic arc. Geodin Acta 19: 251-266 .

Örgün Y, Altınsoy N, Gültekin AH, Karahan G, Celebi N (2005). Natural radioactivity levels in granitic plutons and groundwaters in Southeast part of Eskisehir, Turkey. Appl Radiat Isot 63: 267-275.

Örgün Y, Altınsoy N, Şahin SY, Güngör Y, Gültekin AH, Karahan G, Karacık Z (2007). Natural and anthropogenic radionuclides in rocks and beach sands from Ezine region (Çanakkale), Western Anatolia, Turkey. Appl Radiat Isot 65: 739-747.

Ozgenc I, Ilbeyli N (2008). Petrogenesis of the Late Cenozoic Eğrigöz Pluton in Western Anatolia, Turkey: implications for magma genesis and crustal processes. Int Geol Rev 50: 375-391.

Papadopoulos A, Christofides G, Koroneos A, Papadopoulou L, Papastefanou C, Stoulos S (2013). Natural radioactivity and radiation index of the major granitic plutons in Greece. J Envir Radioact 124: 227-238.

Papadopoulos A, Christofides G, Koroneos A, Stoulos S, Papastefanou C (2012). Natural radioactivity and dose assessment of granitic rocks from Atticocycladic zone (Greece). Period Mineral 81: 301-311.

Pavlidou S, Koroneos A, Papastefanou C, Christofides G, Stoulos S, Vavelides M (2006). Natural radioactivity of granites used as building materials. J Envir Radioact 89: 48-60.

Righi S, Verita S, Bruzzi L, Albertazzi A (2006). Natural radioactivity and radon specific exhalation rate of zircon sands. In: 2nd European IRPA Congress on Radiation Protection, Paris, France.

Robu E, Giovani C (2009). Gamma-ray self-attenuation corrections in environmental samples. Rom Rep Phys 61: 295-300.

Salas HT, Nalini HA Jr, Mendes JC (2006). Radioactivity dosage evaluation of Brazilian ornamental granitic rocks bases on chemical data, with mineralogical and lithological characterization. J Radioanal Nucl Chem 267: 669-673.

Şengör AMC, Yılmaz Y (1981). Tethyan evolution of Turkey: a plate tectonic approach. Tectonophysics 75: 181-241.

Stranden E (1979). Radioactivity of building materials and gamma radiation in dwellings. Phys Med Biol 24: 921-930.

Streckeisen A, Le Maitre RW (1979). A chemical approximation to the modal QAPF classification of the igneous rocks. Egypt Neues Jahrb Mineral Abh 136: 169-206.

Stoulos S, Manolopoulou M, Papastefanou C (2003). Assessment of natural radiation exposure and radon exhalation from building materials in Greece. J Envir Radioact 69: 225-240.

Turhan S (2012). Estimation of possible radiological hazards from natural radioactivity in commercially-utilized ornamental and countertops granite tiles. Ann Nucl Energy 44: 34-39.

Tzortzis M, Tsertos H, Christofides S, Christodoulides G (2003). Gamma measurements and dose rates in commercially used tiling rocks (granites). J Envir Radioact 70: 223-235.

UNSCEAR (1993). United Nations Scientific Committee on the Effects of Atomic Radiation, Exposure from Natural Sources of Radiation. 1993 Report to the General Assembly. New York, NY, USA: UNSCEAR.

UNSCEAR (2000). United Nations Scientific Committee on the Effects of Atomic Radiation. Sources and Effects of Ionising Radiation, Vol. I. New York, NY, USA: UNSCEAR.

UNSCEAR (2006). UNSCEAR 2006 Report Vol. I. Effects of Ionizing Radiation, Report of the General Assemble with Scientific Annexes. New York, NY, USA: UNSCEAR.

WHO (2009). WHO Handbook on Indoor Radon: A Public Health Perspective. Geneva, Switzerland: WHO Press.

Xinwei L, Lingqing W, Xiaodan J (2006). Radiometric analysis of Chinese commercial granites. J Radioanal Nucl Chem 267: 669-673.

Yılmaz Y (1989). An approach to the origin of young volcanic rocks of western Turkey. In: Şengör AMC, editor. Tectonic Evolution of the Tethyan Region. The Hague, the Netherlands: Kluwer Academic, pp. 159-189.

Yılmaz Y, Genç ŞC, Gürer OF, Bozcu M, Yılmaz K, Karacik Z, Altunkaynak Ş, Elmas A, Elmas A (2000). When did the western Anatolian grabens begin to develop? In: Bozkurt E, Winchester JA, Piper JAD, editors. Tectonics and Magmatism in Turkey and the Surrounding Area. London, UK: Geological Society of London Special Publications, pp. 353-384.

Zhang H, Lu Y, Dawson RW, Shi YJ, Wang T (2005). Classification and ordination of DDT and HCH in soil samples from the Guanting Reservoir, China. Chemosphere 60: 762-769.